Chapter in **Advancing Astrophysics with the SKA – II**

Semi-empirical Predictions for Ultra-deep Radio Counts of Star-forming Galaxies with the SKAO

Giulietti Marika,[1] Prandoni Isabella,[1] Bisigello Laura,[2] Bondi Marco,[1] Massardi Marcella,[3] Bonato Matteo[3] and Lapi Andrea[4]

[1]*INAF - Istituto di Radioastronomia, Via Piero Gobetti 101, 40129 Bologna, Italy*

[2]*INAF - Osservatorio Astronomico di Padova, Via dell'Osservatorio 5, 35122 Padova, Italy*

[3]*INAF - Istituto di Radioastronomia - Italian ALMA Regional Centre, Via Gobetti 101, 40129 Bologna, Italy*

[4]*Scuola Internazionale Superiore di Studi Avanzati, Via Bonomea 265, 34136 Trieste, Italy*

E-mail: m.giulietti@ira.inaf.it

Star-forming galaxies (SFGs) dominate the faint radio sky at flux densities below 0.1 mJy. Identifying these systems through a multiwavelength approach is essential to tracing the cosmic history of star formation. Upcoming surveys with the Square Kilometre Array Observatory (SKAO) in its AA4 configuration for the Mid array will probe these faint populations, offering unprecedented insights into the star formation activity of galaxies across cosmic time. Semi-empirical models, built on minimal assumptions and empirical galaxy relations, provide an efficient framework to study galaxy evolution using recent radio and optical/near-infrared (NIR) data. We developed SEMPER (Semi-EMPirical model for Extragalactic Radio emission) to predict the radio luminosity functions and number counts of SFGs. SEMPER combines redshift-dependent stellar mass functions from deep NIR surveys with empirical relations such as the galaxy main sequence and the IR/radio correlation, to characterise the radio properties of massive, high-redshift galaxies. The model shows excellent agreement with recent deep radio observations and naturally predicts a substantial population of massive, dust-obscured galaxies already in place at early epochs. In this chapter, we extend the SEMPER framework to SKA surveys by including an evolving starburst fraction and computing differential number counts at 1.4 GHz for both lensed and unlensed SFGs. Furthermore, we predict the cosmic star formation rate density (SFRD) traced by radio-emitting galaxies up to $z \approx 10$. Our results show that SKA surveys will probe the faintest flux-density regimes, dominated by galaxies powered by star formation, and that <20 hours of SKA-Mid Band 2 observations will recover at least ≈20% of the total SFRD predicted by SEMPER, including contributions from optically/NIR-dark systems up to $z \approx 6$.

1 Introduction

The next generation of radio facilities, led by the Square Kilometre Array Observatory (SKAO), will revolutionise our understanding of galaxy formation and evolution through radio observations. With its unprecedented sensitivity, angular resolution, and survey speed, the SKA will enable the detection of star-forming galaxies (SFGs) out to the epoch of reionisation, providing a dust-unbiased view of the cosmic star formation history.

Over the past decade, deep and wide-area radio surveys conducted with facilities, including SKA precursors and pathfinders, such as the *Karl G. Jansky* Very Large Array (JVLA), LOFAR, ASKAP, and MeerKAT (Helfand et al. 2015; Smolčić et al. 2017; Prandoni et al. 2018; Lacy et al. 2020;Algera et al. 2020; Norris et al. 2021; Heywood et al. 2022; Shimwell et al. 2022) have reached sensitivities deep enough to probe the faint radio population dominated by radio-quiet active galactic nuclei and SFGs (Smolčić et al. 2008; Smolčić et al. 2017; Padovani et al. 2015; Padovani 2016; Prandoni et al. 2018; Algera et al. 2020; van der Vlugt et al. 2021). These surveys have demonstrated the potential of the radio band to complement optical and infrared studies of galaxy evolution, particularly in the most dust-obscured regimes (Smolčić et al. 2017; Best et al. 2023).

Radio emission in SFGs arises from synchrotron radiation, produced by relativistic electrons accelerated in supernova remnants, and from free–free emission in ionised HII regions. This makes radio luminosity a powerful tracer of the star formation rate (SFR), provided that the contribution from AGN is negligible (Condon et al. 2002; Kennicutt and Evans 2012). The tight correlation between radio and far-infrared (FIR) luminosities, the so-called far-infrared/radio correlation (FIRRC; Helou et al. 1985; Condon 1992; Murphy et al. 2011; Delvecchio et al. 2021), further supports the use of radio emission as a dust-independent tracer of star formation activity, even in highly obscured environments.

SKA and its precursor facilities will take this progress to the next level. The planned continuum surveys (Prandoni and Seymour 2015), covering hundreds to thousands of square degrees down to sub–μJy sensitivities, will provide statistically significant samples of SFGs up to redshift $z \gtrsim 10$. These datasets will offer a unique opportunity to test models linking galaxy stellar mass, star formation, and radio emission across cosmic time.

Semi-empirical models provide a powerful way to interpret such forthcoming observations, along with state-of-the-art results from recent facilities, such as *Euclid*, and the James Webb Space Telescope (JWST) in the optical/NIR regime of the electromagnetic spectrum. These models connect key galaxy properties (e.g. stellar mass, SFR, radio luminosity) through empirically calibrated relations, enabling efficient, data-driven predictions while keeping the parameter space limited (Moster et al. 2018; Behroozi et al. 2019; Lapi et al. 2025).

In this work, we employ our Semi-EMPirical model for Extragalactic Radio emission (`SEMPER`; Giulietti et al. 2025) to generate updated predictions for SKAO observations. The model has been successfully tested on radio data at 1.4 GHz and 150 MHz, showing remarkable agreement with the latest determinations from SKA pathfinders such as the Low-Frequency Array (LOFAR, van Haarlem, M. P. et al. 2013) and the Giant Metrewave Radio Telescope (GMRT). Moreover, `SEMPER` can reproduce the observed luminosity functions obtained for samples of radio-selected massive

and dust-obscured SFGs at $z > 3.5$, some of which contain a fraction of optical/NIR dark galaxies (see e.g. Talia et al. 2021; Enia et al. 2022; van der Vlugt et al. 2023), indirectly suggesting a natural link between this population and the radio-bright SFGs population observed at high redshift in deep radio fields. In recent years, several observational studies (e.g. Wang et al. 2019; Gruppioni et al. 2020) have highlighted that this population of dark galaxies can significantly impact the cosmic SFR density (SFRD), with a contribution up to $\approx 40\%$ the contribution of high-redshift Lyman-Break Galaxies (Talia et al. 2021; Enia et al. 2022; Behiri et al. 2023; van der Vlugt et al. 2023; Gentile et al. 2024).

This paper is organised as follows. Section 2 outlines SEMPER and its predictions for the SFRD. In Sect.3, we compare our updated model's number counts at 1.4 GHz with the depths expected for surveys conducted with the SKA-Mid AA4 configuration, along with the predicted SFRD computed from SKA observations. Finally, we summarise our results in Sect. 4. We assume a Chabrier (2003) initial mass function (IMF) and a standard ΛCDM cosmology with parameters: $H_0 = 70\,\mathrm{km\,s^{-1}\,Mpc^{-1}}$, $\Omega_\Lambda = 0.7$ and $\Omega_\mathrm{m} = 0.3$, such that $h_{70} \equiv H_0/(70\,\mathrm{km\,s^{-1}Mpc^{-1}}) = 1$. The radio source spectra are assumed to be described by a simple power law $S_\nu \propto \nu^\alpha$, where S_ν is the monochromatic flux density at a certain frequency ν and α is the radio spectral index.

2 The model

In Giulietti et al. (2025), we presented SEMPER and compared its predictions with the observed luminosity functions and number counts at 1.4 GHz and 150 MHz. In the following, we summarise the main ingredients of the model and the updates introduced in the present analysis.

SEMPER was built by combining up-to-date empirical relations, starting from the redshift-dependent galaxy stellar mass function (SMF), based on the recent deep NIR data from the COSMOS2020 catalogue (Weaver et al. 2023), with up-to-date observed scaling relations: the galaxy main sequence from Popesso et al. (2023) and the mass- and redshift-dependent IRRC from Delvecchio et al. (2021) and McCheyne et al. (2022), drawn at 1.4 GHz and 150 MHz, respectively.

We fitted the SMF for SFGs from the COSMOS2020 catalogue for the redshift range $0.2 \leq z < 5$ along with the local SMF ($z < 0.08$) from Driver et al. (2022). For this purpose, we adopted a double power-law profile, which accounts for the excess of galaxies at high stellar masses for $z \gtrsim$. This approach is analogous to what has been adopted by Shuntov et al. (2025) for SMF obtained from recent JWST observations. The Double Power-law has the form:

$$\log \Phi d \log M_\star = -\log\left(10^{(\log M_\star - \log M_0)(\alpha+1)+\log\Phi_1} + 10^{(\log M_\star - \log M_0)(\beta+1)+\log\Phi_2}\right) d\log M_\star, \tag{1}$$

where $\log\Phi_1$ and $\log\Phi_2$ are the normalisations of the two power laws, α and β are the two slopes, $M_\star$ is the stellar mass, and M_0 represents the mass corresponding to the slope-change. To allow a full interpolation of our model over a broad redshift range, we fitted the best-fitting parameters of the double power-law profile as a function of redshift, enabling us to recover the shape and evolution of the SMFs also in redshift intervals not directly sampled by observations.

The SMFs were then convolved with the main sequence (Brinchmann et al. 2004; Noeske et al. 2007) relation from Popesso et al. (2023). In Giulietti et al. (2025), we assumed SFGs at a fixed redshift and stellar mass to be distributed in SFR as a double Gaussian profile (Béthermin et al. 2012; Sargent et al. 2012; Ilbert et al. 2015; Schreiber et al. 2015). In this assumption, the two Gaussian distributions represent main sequence galaxies, which constitute the dominant population, and starburst galaxies, which are distributed approximately $3-4\sigma$ above the main sequence, and are described as:

$$\begin{aligned}\frac{dp}{d\log\psi}(\psi \mid z, M_\star) = &\left(\frac{A_{\rm MS}}{\sqrt{2\pi\sigma^2_{\rm MS}}}\right)\exp\left[-\frac{(\log\psi - \langle\log\psi\rangle_{\rm MS})^2}{2\sigma^2_{\rm MS}}\right] \\ &+\left(\frac{A_{\rm SB}}{\sqrt{2\pi\sigma^2_{\rm SB}}}\right)\exp\left[-\frac{(\log\psi - \langle\log\psi\rangle_{\rm SB})^2}{2\sigma^2_{\rm SB}}\right].\end{aligned} \tag{2}$$

In the above equation, ψ is the SFR, $\langle\log\psi\rangle_{\rm MS}$ represents the first Gaussian's central value and refers to the main sequence (MS), and $\langle\log\psi\rangle_{\rm SB} = \langle\log\psi\rangle_{\rm MS} + 0.59$ is the central value of the second Gaussian referring to starburst (SB) galaxies. $A_{\rm MS}$ and $A_{\rm SB}$ are the fractions of MS and starburst galaxies, respectively. The one-sigma dispersions of the first and second Gaussians are $\sigma_{\rm MS} = 0.188$ and $\sigma_{\rm SB} = 0.243$. In Giulietti et al. (2025), the starburst fraction $A_{\rm SB}$ was kept fixed at the value of 0.03, following Sargent et al. (2012), assuming therefore this value to remain constant with redshift and stellar mass. In this work, we follow recent results indicating an increase in this quantity, compared to the MS, for low mass ($M_\star \leq 10^9$) or higher redshift ($z \geq 2-3$) galaxies (e.g. Caputi et al. 2017; Bisigello et al. 2018; Chruślińska et al. 2021; Rinaldi et al. 2025). For example, Bisigello et al. (2018) predict the starburst fraction to vary from $\approx 5\%$ at $z = 0.5$–1.0 up to $\approx 16\%$ at $z = 2.0$–3.0 with respect to the total number of galaxies at stellar masses of $\log(M_\star/M_\odot) = 8.25 - 11.25$, while for the low mass regime ($\log(M_\star/M_\odot) < 9$), the number of starburst galaxies varies from $\lesssim 20\%$ at $z \approx 0.75$, and between 20 and 30% at $z \approx 1.5$. Similar results were found in Rinaldi et al. (2025), which extended the redshift range of up to $z \approx 7$, by exploiting JWST data. Therefore, we update our previous prescriptions by also adopting the evolving starburst fractions from Bisigello et al. (2018) and Rinaldi et al. (2025).

The result of the convolution between the SMF and the MS gives the star formation rate function (SFRF):

$$\frac{d^2N_{\rm SMF+MS}}{d\log\psi\, dV}(z, \log\psi) = \int d\log M_\star \frac{d^2N_{\rm SFG}}{d\log M_\star dV}(z, \log M_\star) \times \frac{dp}{d\log\psi}(\log\psi \mid z, M_\star), \tag{3}$$

where V is the comoving cosmological volume.

2.1 Radio Luminosity Function and Number Counts

The radio luminosity function (LF) for SFGs can be derived by expressing the SFRF in terms of the radio luminosity L_ν at a given frequency ν. For this purpose, we adopted the stellar mass- and

redshift-dependent $L_{\rm SFR}$–radio correlation from Delvecchio et al. (2021), defined by the parameter $q_{\rm UV+IR}$:

$$q_{\rm UV+IR}(M_\star, z) = (2.743 \pm 0.034) \times A^{(-0.025\pm0.012)} - B \times (0.234 \pm 0.017). \tag{4}$$

Where $A = (1 + z)$, $B = \log(M_\star/M_\odot) - 10$. $q_{\rm UV+IR} = q_{\rm SFR}$ includes the contribution for the dust-uncorrected UV emission (see Sec. 2.3 of Giulietti et al. 2025 for details) and is expressed as:

$$q_{\rm UV+IR} = \log\left(\frac{L_{\rm SFR}[\rm W]/3.75 \times 10^{12}}{L_{\rm 1.4GHz}\left[\rm W\,Hz^{-1}\right]}\right). \tag{5}$$

In the above expression, $L_{\rm 1.4GHz}$ is the rest-frame radio luminosity at 1.4 GHz, and $L_{\rm SFR}$ is the luminosity obtained from ψ using the relations from Kennicutt and Evans (2012) rescaled to a Chabrier (2003) IMF.

We then combined Eqs. 4, 5, and 6 with Eq. 3 and convolved the result with a Gaussian distribution representing the probability of having a given radio luminosity at the frequency ν (L_ν), at fixed ψ, $M_\star$ and z:

$$\frac{d\rm p}{d\log L_\nu}(\log L_\nu \mid \psi, M_\star, z) = \left(\frac{1}{\sqrt{2\pi\sigma^2_{\rm q_{UV+IR}}}}\right)\exp\left[-\frac{(\log L_\nu - \langle\log L_\nu\rangle)^2}{2\sigma^2_{\rm q_{UV+IR}}}\right]. \tag{6}$$

The term $\sigma_{\rm UV+IR}$ accounts for the scatter of Eq. 4 and $\langle\log L_\nu\rangle$ is the radio luminosity corresponding to a given ψ, and it is derived from Eq. 5 by rescaling the frequency ν from 1.4 GHz. The final expression for the LF of SFGs, obtained by combining Eq. 3, with Eq. 5 and Eq. 6, is:

$$\begin{aligned}\frac{d^2\rm N}{d\log L_\nu dV}(\log L_\nu, z) = \int d\log M_\star \frac{d^2 N_{\rm SFG}}{d\log M_\star dV}(\log M_\star \mid z) \\ \times \int d\log\psi \frac{dp}{d\log\psi}(\psi \mid z, M_\star) \\ \times \frac{d\rm p}{d\log L_\nu}(\log L_\nu \mid \psi, M_\star, z)\,.\end{aligned} \tag{7}$$

By integrating the above equation over the redshift, one obtains:

$$\frac{d^2 N}{d\log S_\nu d\Omega}(S_\nu) = \int dz \frac{d^2 V}{dz d\Omega}\frac{d^2 N}{d\log L_\nu dV}\left(L_{\nu(1+z)}, z\right), \tag{8}$$

which is the expression for the radio-band number counts. $dV/dzd\Omega$ is the cosmological volume per unit solid angle, and S_ν is the observed flux defined as:

$$S_\nu = \frac{L_{\nu(1+z)}(1+z)}{4\pi D_L^2(z)}, \tag{9}$$

with $D_L(z)$ being the luminosity distance.

Mancuso et al. (2017) found that strongly lensed SFGs at high redshift contribute about 1% to the radio number counts at $S_{1.4\,\mathrm{GHz}} \approx 0.5\,\mathrm{mJy}$. Therefore, we also compute the number counts for strongly lensed SFGs by accounting for the probability distribution of the magnification $dp/d\mu$ derived by Lapi et al. (2012). The differential number counts for galaxy–galaxy lensing in the radio band are expressed as:

$$\frac{dN^2_{\mathrm{lens}}}{d\log S_\nu d\Omega}(S_\nu) = \int dz_s \frac{1}{\langle\mu\rangle} \int^{\mu_{\mathrm{max}}} d\mu \frac{dp}{d\mu} \frac{d^2N}{d\log S_\nu d\Omega}(S_\nu/\mu)\,, \tag{10}$$

where z_s is the redshift of the lensed galaxy, μ is the magnification factor. Here, we assume $\mu_{\mathrm{max}} \approx 25$ for sources extended up to a few kiloparsecs, and $<\mu>$ is approximated as unity for the case of large-area surveys. The resulting number counts are shown in Fig. 1.

2.2 The Cosmic Star Formation Rate Density

We can exploit `SEMPER` to make predictions on the evolution of the Cosmic SFRD. Given the SFRF, the SFRD (ρ_ψ) can be computed as:

$$\rho_\psi(z) = \int d\log\psi\, \psi \frac{d^2N}{d\log\psi dV}(\psi, z). \tag{11}$$

By substituting Eq. 3, one obtains:

$$\frac{d\rho}{d\log M_\star}(z|M_\star) = \left(\int d\log\psi\, \psi \frac{dp}{d\log\psi}\right) \times \frac{d^2N_{\mathrm{SFG}}}{d\log M_\star dV}(z, \log M_\star). \tag{12}$$

3 Predictions for Square Kilometre Array's surveys

The SKA-Mid AA4 configuration will consist of 197 dishes operating across five frequency bands. The range spanning approximately 1 and 1.4 GHz, corresponding to bands 1 and 2 of SKA-Mid, has been selected for several planned surveys (Prandoni and Seymour, 2015, and see also Prandoni et al. 2026 in this volume). Surveys with galaxy and AGN co-evolution as science driver are divided into Ultra-Deep, Deep, and Wide, covering areas of 1 deg^2, 10–30 deg^2, and about 10^3 deg^2. These surveys reach rms sensitivities of 0.05 µJy, 0.2 µJy, and 1 µJy rms, respectively, corresponding to continuum integration times of approximately 2267, 167, and 6.7 hrs per pointing, adopting a Briggs weighting scheme for the AA4 configuration (see Prandoni et al. 2026 in this volume for details). For the same rms sensitivities, but adopting the AA* configuration, the continuum integration times correspond to 11 111, 698, 28 hrs. Confusion limit affects only the Ultra-Deep survey, and a minimum angular resolution of 2 arcseconds is required for the AA* configuration to avoid it. In Fig. 1, we report the radio number counts for unlensed and lensed SFGs at 1.4 GHz predicted by our model, along with the 5σ limits for the three SKA-Mid surveys shown as dashed (dotted) vertical lines for the AA4 (AA*) configuration. Our results are compared with

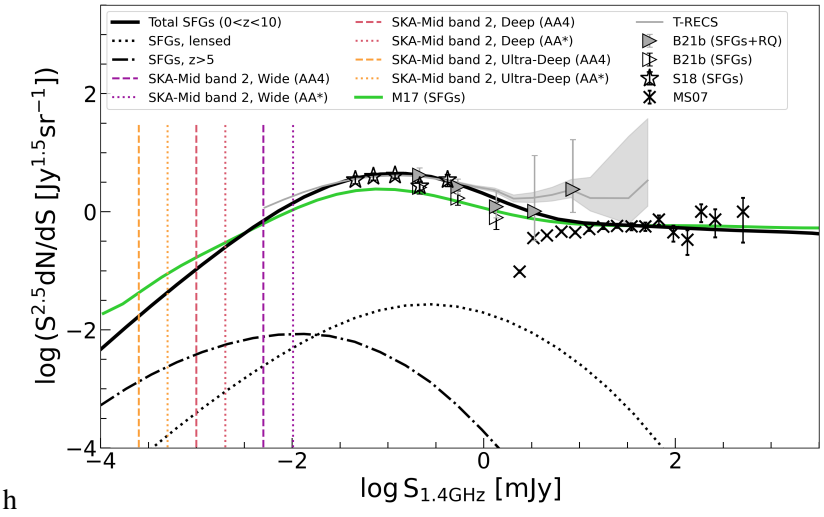

Figure 1: Euclidean normalised differential number counts from SEMPER for total (black solid line), high-z ($5 \leq z \leq 10$, dashdotted line), and lensed SFGs (black dotted line) at 1.4 GHz. The solid green line is the prediction from Mancuso et al. (2017). Triangles are data from Bonato et al. (2021) for SFGs (empty) and SFGs and RQ sources combined (grey filled). Black crosses show the number counts for local galaxies from Mauch and Sadler (2007). Stars mark the SFGs from Seymour et al. (2008). The grey shaded area displays the predictions from the T-RECS simulation by Bonaldi et al. (2019, 2023). The dashed and dotted vertical lines represent the 5σ limits for the three SKA-Mid Band 2 surveys adopting the AA4 and AA* configuration, respectively.

observations of SFGs from Mauch and Sadler (2007), Seymour et al. (2008), and Bonato et al. (2021), with the T-RECS simulation (Bonaldi et al. 2019, 2023), and with the semi-empirical model from Mancuso et al. (2017). The SKA-Mid Band 2 Wide survey conducted with the AA* configuration will reach an rms sensitivity of 2 µJy, enabling the detection of SFGs up to $z \approx 10$ at 5σ, corresponding to flux densities about 0.6 dex fainter than those currently observed. With the more extended AA4 configuration, the survey will push the detection limit down to ≈1 dex fainter than current observations for SFGs. In particular, we predict at least $\approx 3 \times 10^4$ SFGs up to z≈ 10 per square degree for the wide survey. For comparison, a deep radio survey at a similar frequency, such as the COSMOS-VLA 3 GHz Large Project (see e.g. Novak et al. 2017) obtained with 384 hours of observations, found ≈ 6000 SFGs up to $z \approx 5$ over 2 deg^2 with flux densities higher than 11.5 µJy. Moreover, we predict 5136, 1364, and 232 SFGs at $5 \leq z \leq 10$ at $S_{1.4\,\mathrm{GHz}} > 0.25$ µJy, 1.0 µJy and 5.0 µJy, corresponding to the 5σ depth of the SKA-Mid Ultra-Deep, Deep, and Wide surveys, respectively (see Fig. 2). For the same depths, we predict 489, 275, and 124 strongly lensed SFGs. Moreover, we estimate that lensed sources contribute approximately 0.6% to the total counts of SFGs.

In Fig. 3 we show the Cosmic SFRD predicted by our model, along with the contribution provided by SKA-Mid Band 2 at a 5σ flux limit for the Ultra-Deep, Deep, and Mid surveys. We compare our predictions with results from various multi-band surveys conducted at different wavelengths.

We estimate that, with less than 20 hours of SKA-Mid Band 2 observations using the AA4 configuration, we can detect at least 20% of the total SFRD predicted by SEMPER, including the contribution

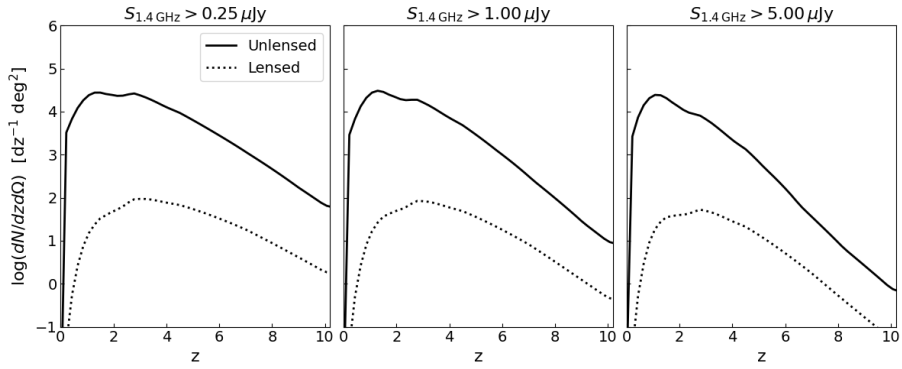

Figure 2: Predicted redshift distributions of the unlensed and lensed SFGs for the three SKA-Mid Band 2 surveys, computed adopting 5σ flux limits.

from dark galaxies up to redshift ≈ 6 (see e.g. Talia et al. 2021, Enia et al. 2022, Gentile et al. 2024, 2025). For reference, the selections presented by Talia et al. (2021) and Gentile et al. (2024) identified about 300 NIR-dark galaxies within the COSMOS-VLA 3,GHz Large Project, out of a parent sample of $\gtrsim$ 6000 SFGs over approximately 2 deg^2. According to our predictions for the planned SKA-Mid Band 2 surveys, more than $\approx$ 1500 dark sources per deg^2 are expected above 5 µJy at 1.4 GHz. This corresponds to a substantial increase in the number statistics compared to current deep radio surveys, enabling the construction of significantly larger and more representative samples of dust-obscured systems. In addition to sensitivity, the wide sky coverage of the planned SKA surveys will strongly mitigate cosmic variance, which currently limits studies of rare, massive, dust-enshrouded galaxies. Importantly, the SFRD fraction probed at these flux limits coincides with the regime where obscured star formation is expected to provide a significant contribution to the total cosmic SFR budget at high redshift. SKA observations will therefore allow a direct determination of the obscured component of the SFRD and offer the possibility to distinguish between different evolutionary scenarios for massive SFGs at $z > 3$.

4 Conclusions

We presented an updated version of the Semi-EMPirical model for Extragalactic Radio emission (`SEMPER`, Giulietti et al. 2025) and provided predictions for planned SKA surveys (Prandoni and Seymour, 2015). In particular, we computed the differential number counts at 1.4 GHz for lensed and unlensed SFGs and the cosmic star formation rate density (SFRD) up to redshift $\approx$ 10 for radio-bright SFGs. SKA surveys will probe the faintest flux density regimes ($S_{1.4\,\mathrm{GHz}} < 0.1$ mJy), corresponding to a range dominated by galaxies whose radio emission arises primarily from star formation, and will account for a significant number of high-z ($5 \leq z \leq 10$) SFGs ($\gtrsim$ 200) and strongly lensed SFGs ($\gtrsim$ 100). We also showed that at least $\approx$ 20% of the total SFRD predicted by `SEMPER` can be recovered with $\lesssim$20 hours of SKA-Mid Band 2 observations, including contributions from the observed optically/NIR-dark galaxies up to z$\approx$6. Our model serves as a bridge between existing deep surveys and the upcoming SKA era, offering predictions for the evolution of radio emission in SFGs throughout cosmic time, which will be tested with future observations.

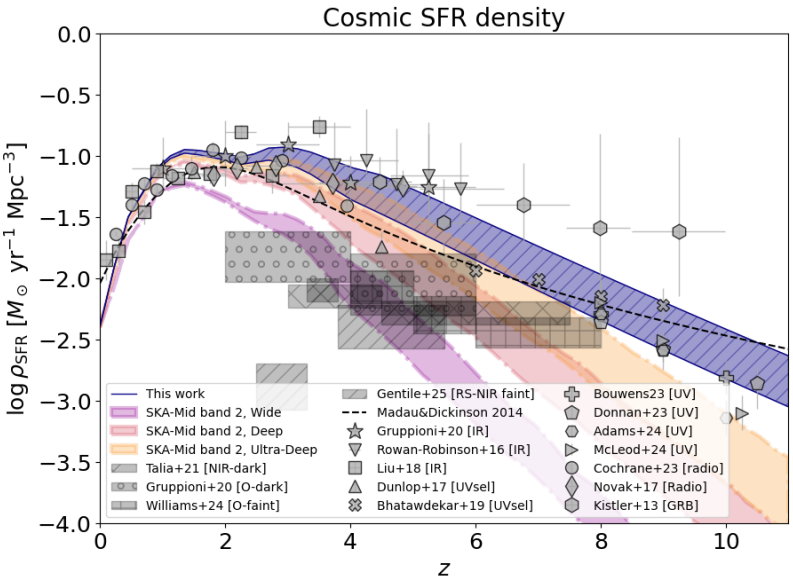

Figure 3: Predictions from SEMPER for the Cosmic SFRD compared with results from various multi-band surveys. The blue-hatched area represents the total contribution from SFGs as predicted by our model. The purple, red, and orange areas represent SEMPER's predictions for the SKA-Mid Band 2 surveys at a 5σ flux limit. The lower limit of each area represents the minimum fiducial value of the SFRD from our model, while the scatter reflects the uncertainty in the starburst fraction at low masses. For each prediction, the width of the coloured area reflects the range of starburst fractions assumed in the model. Data are from Kistler et al. (2013, hexagons), Rowan-Robinson et al. (2016, inverse triangles), Dunlop et al. (2017, triangles), Novak et al. (2017, rhomboids), Liu et al. (2018, squares), Bhatawdekar et al. (2019, crosses), Gruppioni et al. (2020, stars), Bouwens et al. (2023, plus signs), Cochrane et al. (2023, circles), Donnan et al. (2023, pentagons), Adams et al. (2024, rotated hexagons), and McLeod et al. (2024, rotated triangles). Data referring to high-z dusty galaxies are from Gruppioni et al. (2020, grey shaded area hatched with circles; IR-selected HST-dark sources), Talia et al. (2021, grey shaded area hatched with crosses; radio-selected NIR-dark sources), Gentile et al. (2025, grey shaded area hatched with stars; radio-selected NIR-faint sources observed with JWST), and Williams et al. (2024, grey shaded area hatched with plus signs; O-dark sources observed with JWST). The dashed line is from Madau and Dickinson (2014).

Acknowledgements

We acknowledge support from INAF under the following funding schemes: Large Grant 2022 (project "MeerKAT and LOFAR team up: a Unique Radio Window on Galaxy/AGN co-Evolution") and Large GO 2024 (project "MeerKAT and Euclid Team up: Exploring the galaxy-halo connection at cosmic noon"). Part of the research activities described in this paper were carried out with contribution of the Next Generation EU funds within the National Recovery and Resilience Plan (PNRR), Mission 4 - Education and Research, Component 2 - From Research to Business (M4C2), Investment Line 3.1 - Strengthening and creation of Research Infrastructures, Project IR0000034 – "STILES - Strengthening the Italian Leadership in ELT and SKA".

References

N. J. Adams et al. *ApJ*, 965(2):169, Apr. 2024. doi: 10.3847/1538-4357/ad2a7b.
H. S. B. Algera et al. *ApJ*, 903(2):139, Nov. 2020. doi: 10.3847/1538-4357/abb77a.
M. Behiri et al. *ApJ*, 957(2):63, Nov. 2023. doi: 10.3847/1538-4357/acf616.
P. Behroozi, R. H. Wechsler, A. P. Hearin, and C. Conroy. *MNRAS*, 488(3):3143–3194, Sept. 2019. doi: 10.1093/mnras/stz1182.
P. N. Best et al. *MNRAS*, 523(2):1729–1755, Aug. 2023. doi: 10.1093/mnras/stad1308.
M. Béthermin et al. *ApJL*, 757(2):L23, Oct. 2012. doi: 10.1088/2041-8205/757/2/L23.
R. Bhatawdekar, C. J. Conselice, B. Margalef-Bentabol, and K. Duncan. *MNRAS*, 486(3):3805–3830, July 2019. doi: 10.1093/mnras/stz866.
L. Bisigello, K. I. Caputi, N. Grogin, and A. Koekemoer. *A&A*, 609:A82, Jan. 2018. doi: 10.1051/0004-6361/201731399.
A. Bonaldi et al. *MNRAS*, 482(1):2–19, Jan. 2019. doi: 10.1093/mnras/sty2603.
A. Bonaldi et al. *MNRAS*, 524(1):993–1007, Sept. 2023. doi: 10.1093/mnras/stad1913.
M. Bonato et al. *MNRAS*, 500(1):22–33, Jan. 2021. doi: 10.1093/mnras/staa3218.
R. J. Bouwens et al. *MNRAS*, 523(1):1036–1055, July 2023. doi: 10.1093/mnras/stad1145.
J. Brinchmann et al. *MNRAS*, 351(4):1151–1179, July 2004. doi: 10.1111/j.1365-2966.2004.07881.x.
K. I. Caputi et al. *ApJ*, 849(1):45, Nov. 2017. doi: 10.3847/1538-4357/aa901e.
G. Chabrier. *PASP*, 115(809):763–795, July 2003. doi: 10.1086/376392.
M. Chruślińska, G. Nelemans, L. Boco, and A. Lapi. *MNRAS*, 508(4):4994–5027, Dec. 2021. doi: 10.1093/mnras/stab2690.
R. K. Cochrane et al. *MNRAS*, 523(4):6082–6102, Aug. 2023. doi: 10.1093/mnras/stad1602.
J. J. Condon. *ARA&A*, 30:575–611, Jan. 1992. doi: 10.1146/annurev.aa.30.090192.003043.
J. J. Condon, W. D. Cotton, and J. J. Broderick. *AJ*, 124(2):675–689, Aug. 2002. doi: 10.1086/341650.
I. Delvecchio et al. *A&A*, 647:A123, Mar. 2021. doi: 10.1051/0004-6361/202039647.
C. T. Donnan et al. *MNRAS*, 518(4):6011–6040, Feb. 2023. doi: 10.1093/mnras/stac3472.
S. P. Driver et al. *MNRAS*, 513(1):439–467, June 2022. doi: 10.1093/mnras/stac472.
J. S. Dunlop et al. *MNRAS*, 466(1):861–883, Apr. 2017. doi: 10.1093/mnras/stw3088.
A. Enia et al. *ApJ*, 927(2):204, Mar. 2022. doi: 10.3847/1538-4357/ac51ca.
F. Gentile et al. *ApJ*, 962(1):26, Feb. 2024. doi: 10.3847/1538-4357/ad1519.
F. Gentile et al. *A&A*, 697:A46, May 2025. doi: 10.1051/0004-6361/202452461.
M. Giulietti et al. A&A, 697:A81, May 2025. doi: 10.1051/0004-6361/202453331.
C. Gruppioni et al. *A&A*, 643:A8, Nov. 2020. doi: 10.1051/0004-6361/202038487.
D. J. Helfand, R. L. White, and R. H. Becker. *ApJ*, 801(1):26, Mar. 2015. doi: 10.1088/0004-637X/801/1/26.
G. Helou, B. T. Soifer, and M. Rowan-Robinson. *ApJL*, 298:L7–L11, Nov. 1985. doi: 10.1086/184556.
I. Heywood et al. *MNRAS*, 509(2):2150–2168, Jan. 2022. doi: 10.1093/mnras/stab3021.
O. Ilbert et al. *A&A*, 579:A2, July 2015. doi: 10.1051/0004-6361/201425176.
R. C. Kennicutt and N. J. Evans. *ARA&A*, 50:531–608, Sept. 2012. doi: 10.1146/

annurev-astro-081811-125610.
M. D. Kistler, H. Yuksel, and A. M. Hopkins. *arXiv e-prints*, art. arXiv:1305.1630, May 2013. doi: 10.48550/arXiv.1305.1630.
M. Lacy et al. *PASP*, 132(1009):035001, Mar. 2020. doi: 10.1088/1538-3873/ab63eb.
A. Lapi et al. *ApJ*, 755(1):46, Aug. 2012. doi: 10.1088/0004-637X/755/1/46.
A. Lapi, L. Boco, and F. Shankar. *Encyclopedia of Astrophysics, Elsevier, in press*, art. arXiv:2502.12764, Feb. 2025. doi: 10.48550/arXiv.2502.12764.
D. Liu et al. *ApJ*, 853(2):172, Feb. 2018. doi: 10.3847/1538-4357/aaa600.
P. Madau and M. Dickinson. *ARA&A*, 52:415–486, Aug. 2014. doi: 10.1146/annurev-astro-081811-125615.
C. Mancuso et al. *ApJ*, 842(2):95, June 2017. doi: 10.3847/1538-4357/aa745d.
T. Mauch and E. M. Sadler. *MNRAS*, 375(3):931–950, Mar. 2007. doi: 10.1111/j.1365-2966.2006.11353.x.
I. McCheyne et al. *A&A*, 662:A100, June 2022. doi: 10.1051/0004-6361/202141307.
D. J. McLeod et al. *MNRAS*, 527(3):5004–5022, Jan. 2024. doi: 10.1093/mnras/stad3471.
B. P. Moster, T. Naab, and S. D. M. White. *MNRAS*, 477(2):1822–1852, June 2018. doi: 10.1093/mnras/sty655.
E. J. Murphy et al. *ApJ*, 737(2):67, Aug. 2011. doi: 10.1088/0004-637X/737/2/67.
K. G. Noeske et al. *ApJL*, 660(1):L43–L46, May 2007. doi: 10.1086/517926.
R. P. Norris et al. *PASA*, 38:e046, Sept. 2021. doi: 10.1017/pasa.2021.42.
M. Novak et al. *A&A*, 602:A5, June 2017. doi: 10.1051/0004-6361/201629436.
P. Padovani. *A&ARv*, 24(1):13, Sept. 2016. doi: 10.1007/s00159-016-0098-6.
P. Padovani et al. *MNRAS*, 452(2):1263–1279, Sept. 2015. doi: 10.1093/mnras/stv1375.
P. Popesso et al. *MNRAS*, 519(1):1526–1544, Feb. 2023. doi: 10.1093/mnras/stac3214.
I. Prandoni and N. Seymour. In *Advancing Astrophysics with the Square Kilometre Array (AASKA14)*, page 67, Apr. 2015. doi: 10.22323/1.215.0067.
I. Prandoni et al. *MNRAS*, 481(4):4548–4565, Dec. 2018. doi: 10.1093/mnras/sty2521.
I. Prandoni et al. In *Advancing Astrophysics with the SKA – II (AASKAII)*. 2026. arXiv search: Report number AASKAII/Prandoni01.
P. Rinaldi et al. *ApJ*, 981(2):161, Mar. 2025. doi: 10.3847/1538-4357/adb309.
M. Rowan-Robinson et al. *MNRAS*, 461(1):1100–1111, Sept. 2016. doi: 10.1093/mnras/stw1169.
M. T. Sargent, M. Béthermin, E. Daddi, and D. Elbaz. *ApJL*, 747(2):L31, Mar. 2012. doi: 10.1088/2041-8205/747/2/L31.
C. Schreiber et al. *A&A*, 575:A74, Mar. 2015. doi: 10.1051/0004-6361/201425017.
N. Seymour et al. *MNRAS*, 386(3):1695–1708, May 2008. doi: 10.1111/j.1365-2966.2008.13166.x.
T. W. Shimwell et al. *A&A*, 659:A1, Mar. 2022. doi: 10.1051/0004-6361/202142484.
M. Shuntov et al. *A&A*, 695:A20, Mar. 2025. doi: 10.1051/0004-6361/202452570.
V. Smolčić et al. *A&A*, 602:A1, June 2017. doi: 10.1051/0004-6361/201628704.
V. Smolčić et al. *The Astrophysical Journal Supplement Series*, 177(1):14, jul 2008. doi: 10.1086/588028.
M. Talia et al. *ApJ*, 909(1):23, Mar. 2021. doi: 10.3847/1538-4357/abd6e3.
D. van der Vlugt et al. *ApJ*, 907(1):5, Jan. 2021. doi: 10.3847/1538-4357/abcaa3.
D. van der Vlugt et al. *ApJ*, 951(2):131, July 2023. doi: 10.3847/1538-4357/acd549.

van Haarlem, M. P. et al. *A&A*, 556:A2, 2013. doi: 10.1051/0004-6361/201220873.
L. Wang et al. *A&A*, 631:A109, Nov. 2019. doi: 10.1051/0004-6361/201935913.
J. R. Weaver et al. *A&A*, 677:A184, Sept. 2023. doi: 10.1051/0004-6361/202245581.
C. C. Williams et al. *ApJ*, 968(1):34, June 2024. doi: 10.3847/1538-4357/ad3f17.